Study of the thermal behaviour of a derivative based on a zirconium agent (modified montmorillonite) and determination of the physical characteristics

Zoulikha Khiati [1] & Lahouari Mrah*[,2,3]

[1]Département de chimie-physique, Faculté de chimie, Université des Sciences et de la Technologie d'Oran, M. Boudiaf,
BP 1505 El M'naouar, 31000 Oran, Algeria

[2]Laboratoire de Chimie des Polymères (LCP), Faculté des sciences exactes et appliquées, Université Oran1 Ahmed Ben Bella,
BP 1524, El Mnaouar 31000, Oran, Algérie

[3]Ecole Supérieure en Génie Electrique et Energétique d'Oran, Chemin Vinical N°9, Oran, Algerié (ESGEE)

E-mail : lmrah@yahoo.fr

In this research, untreated Algerian maghnite has been used to develop two types of modified clays: the first one is a homo-ionic sodium clay (Na-Mag) which is a support to develop a montmorillonite by insertion of zirconium hydroxyl cations. The different series of techniques, including thermogravimetric analysis (TGA), differential thermal analysis (DTA), dynamic light scattering (DLS), and zeta potential (ζ), have been used to define the physical characteristics of the clays by studying their particle size distribution as well as the thermal profile. In addition, the pillar-shaped montmorillonite (Maghnite) exhibit a negative charge even when its *p*H reach 2.8. This large negative surface charge of montmorillonite suggests optimal removal of organic molecule particles present in the aqueous medium. The results obtained by Fourier transform infrared (FT-IR) analysis show that the bands characterizing the presence of intercalating agents are visible. Thermography of the zirconium pillar species shows an improvement in the thermal stability of the silicate structure with two well differentiated zones. Adsorbed organic cations result in a reduction of the surface load, that is, a decrease of its negativity, as well as a cancellation of the charge.
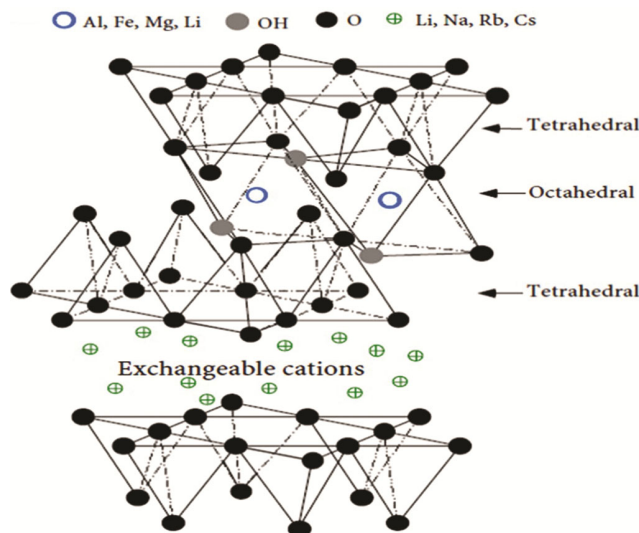
Keywords: Dynamic light scattering (DLS), Maghnite, Pillared clays, Silicate structure, Zeta-potential (ζ)

In Algeria, the most economically important montmorillonite deposits are in Oranie (western Algeria). are in Oranie (western Algeria). One notes in particular the quarry of Maghnia (Hammam Boughrara) whose reserves are estimated at two million tons. This Algerian clay, known as Maghnite, has been studied and characterized by many research works[1-3]. Table 1 shows its elemental chemical composition. Maghnite contains mainly SiO_2 followed by Al_2O_3 (Ref. 4) (Scheme 1), hence its belonging to the alumino-silicate family. Various analyses carried out show that maghnite contains a large proportion of montmorillonite, quartz, cristobalite, calcite and other minerals. Maghnite has been used since its appearance as a catalyst and also as a reinforcement in the synthesis of composite polymers. The family of pillar clays is very recent. They are two-dimensional materials with a porous texture and a structure capable of being used for adsorption and catalysis. The preparation of clays generally involves ion exchange of interlayer region cations by inorganic polyoxycations that subsequently convert to oxides to yield a microporous material that can become a molecular sieve[5]. For piling, the polynuclear hydroxyzirconium complex, whose structure is shown below, is one of the most commonly used cations to date. $[Zr_4 (OH)_{14} (H_2O)_{10}]_2^+$ (Refs 6,7). Adsorbed organic cations attenuate the surface loading, which result in a reversal of loading[8,9]. As a result, the adsorption of organic cations is evaluated by measuring the change in the zeta potential (ξ) of the clay surface, a relatively measure that provides the stability of the organic clay in dispersion. The potential (ξ) existing between the slip plane and the bulk solution is a significant electrokinetic feature in the case of clay minerals. This property has been applied to measure the stability of clay dispersions[10,11], and to describe the aggregation, flow, sequestration, and filtration of clay[12]. The determination of the characteristics (ξ) reveal both the stability of colloids, the mode of adsorption of both inorganic and organic molecules at the solid/solution interface. In this

Table 1 — Chemical structure of maghnite[13]								
Species	SiO_2	Al_2O_3	Fe_2O_3	Na_2O	K_2O	CaO	MgO	TiO_2	SO_3
(%)wt	69,39	14,67	1,16	0,5	0,79	0,3	1,07	0,16	0,91

Scheme 1 —Configuration of the maghnite network

research, we evaluated the different electrokinetic properties of the Maghnite surface through the microelectrophoresis procedure. The results of the work highlight the value of these materials for a specific use in the industry.

Experimental Section

Materials

The clay material used in this study was extracted in the raw state by ENOF Bental Spa of the Compagnie Nationale de Fabrication de Produits Miniers Non-Ferrous, Maghnia (Algeria) and used without further purification. The chemical formula of this clay mineral is as follows: $[Si_{7.89}\ Al_{3.34}\ Fe_{0.42}Mg_{0.56}\ Ca_{0.52}\ Na_{0.14}\ K_{0.01}$ (Ref. 14)]. Its cationic exchange capacity (CEC) is reported to be around 90 meq.100g^{-1} (Ref. 15). Following the usual procedure described above, the homoionic clay was developed by an ion exchange between Montmorillonite (Maghnite) and NaCl (Ref. 16,17). The chemicals used in this study, including NaCl, $ZrOCl_2.8H_2O$, HCl, and NaOH, NaCl, were selected as analytical grade reagents from the Guangzhou Chemical Reagent Plant (Guangdong Province, China).

Zr-Maghnite (Zr-Mag) was prepared by ion exchange between Na-Mag and zirconium agent. The Na-Mag suspension (20 g in 100 mL of distilled water) was thus treated with a solution of $ZrOCl_2$ $8H_2O$ (0.1 M, 100 mL) and then kept under magnetic stirring for 6 hours at room temperature. At the end of this exchange process, a suspension was subjected to filtration and rinsed several times with distilled water. The powder was then dried under vacuum at 110 °C and finally designated as Zr-Mag[18].

Characterization

Diffraction analysis (DRX) was made at room temperature by Bruker D8 Advance X-Ray diffractometer (40 kV, 30 mA) by means of CuKα radiation (λ = 0.154 nm) . IR analyses of Na-Maghnite, Zr-Maghnite were done using Perkin-Elmer Spectrum Two FT-IR with UATR sample attachment. The curves were recorded using a thermogravimetric instrument of the PerkinElmer type (TGA4000). Maghnite samples were analyzed at a heating rate of at a heating rate of 10°C / min under a nitrogen purge at a flow rate of 50 mL / min and with a temperature sweep from 30 to 880°C. Differential scanning calorimetry (DSC) is performed on a Mettler TA 4000 in an aluminum crucible. The heating rate is 5K/min. The verification of the measurements made on the diameter of the products in the range 1-900 nm was obtained using the dynamic light diffusion technique. (Zetasizer Nano, ZS, HORIBA). Prior to examinations, the clay suspension is prepared by sonication and stored in distilled water for up to 48 hours. The values of the zeta potential of the prepared suspensions (1.5g.L^{-1}) were obtained at various pH values to define the zero load points. The surface morphologies of all the developed components were examined by scanning electron microscopy (SEM) "JEOL 7001F, FEG-SEM". Transmission electron micrographs (TEM) were executed on a Hitachi 8100 type device.

Results and Discussion

FTIR analysis

Figure 1 shows the FTIR spectrum of each of the samples. This figure shows both the intensity and the degree of water adsorption for the different clays studied. According to Fig. 1, a band located at 3618 cm^{-1} which is attributed to the specific O-H vibration of the silicate. We can also distinguish the presence of an O-H vibration of the adsorbed water molecules in the central part of the clay at 3426 cm^{-1}, while the
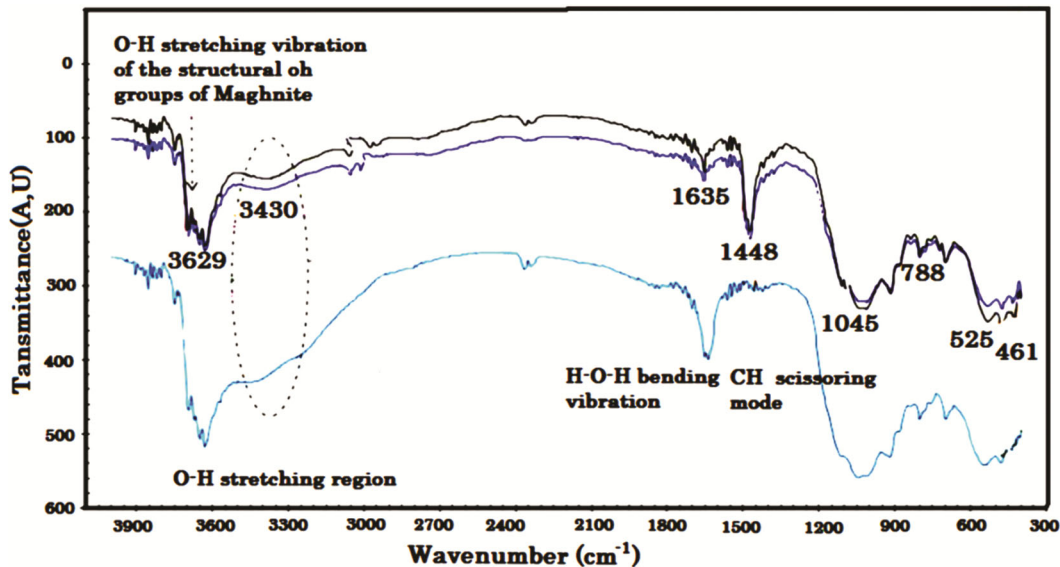
Fig. 1 — FTIR curves of the Mt and Zr-Mag

bending vibrations observed at 1637 cm^{-1} are related to the characteristic vibration that constitutes the silica in its structure[19]. This band gradually shifts as the zirconium silicate concentration increases, reaching a value of 1637 cm^{-1}. From the data presented in Figure 1, there is a peak located at 1045 cm^{-1} corresponding to the stretching vibration of the Si-O bond. On the other hand, a band is recorded at 612 cm^{-1} associated with coupled Al-O and Si-O out-of-plane vibrations[20]. After the intercalation of the zirconium agent in Na-Maghnite, new infrared adsorption bands appear and it is clear that the band centered at 3426 cm^{-1} has a higher frequency than the base clay (Maghnite) due to the presence of hydroxyl groups of the zirconium agent as well as hydroxyl groups involved in the hydrogen-water bonding. Simultaneously, the peak corresponding to the bending vibration of water molecules located at 1637 cm^{-1} was also increased in intensity[21].

X-ray diffraction analyses

Figure 2 shows the diffractograms of sodium Maghnite (Na-Mag) and Modified Maghnite (Zr-Mag).

Na-Mag shows a peak at $2\theta=7.0°$ corresponding to an interfoliar distance $d_{001}=15.22$ Å. The incorporation of zirconium oxychloride ions reveals a peak located at $2\theta=4.5°$, which may be due to a heterogeneous organization (dispersion) of the Maghnite sheets, hence the possibility of the presence of a group of sheets separated by a distance $d_{001}=18.35A°$. The increase of this distance indicates that there is an intercalation of the ions in the
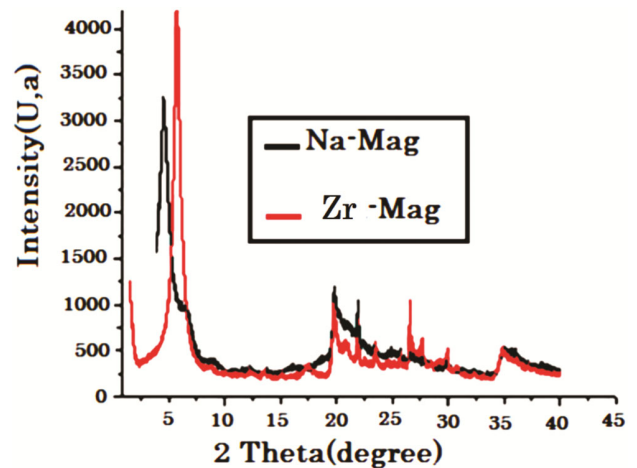

Fig. 2 — X-ray diffraction patterns of a) Na-Mag and b) Zr- Mag.

interfoliar galleries of the Na-Mag by a simple cationic exchange and a simple cationic exchange and a flocculation of the intercalated sheets thanks to interactions between the sheets of Maghnite. After reaction with zirconium oxychloride, the interlayer spacing of Zr-Mag samples increases to 16.05 Å due to the presence of zirconium pillar species (Fig.2)[22,23]. These data are consistent with those reported in the literature for Zr pillared clays. [24]

Transmission electronic microscopy

To substantiate the X-ray diffraction results, Na-Mag and its counterpart Zr-Mag were examined by Transimission electron microscopy "TEM" as shown in Fig. 3. The TEM images taken on Na-Mag show a remotely homogeneous structure,
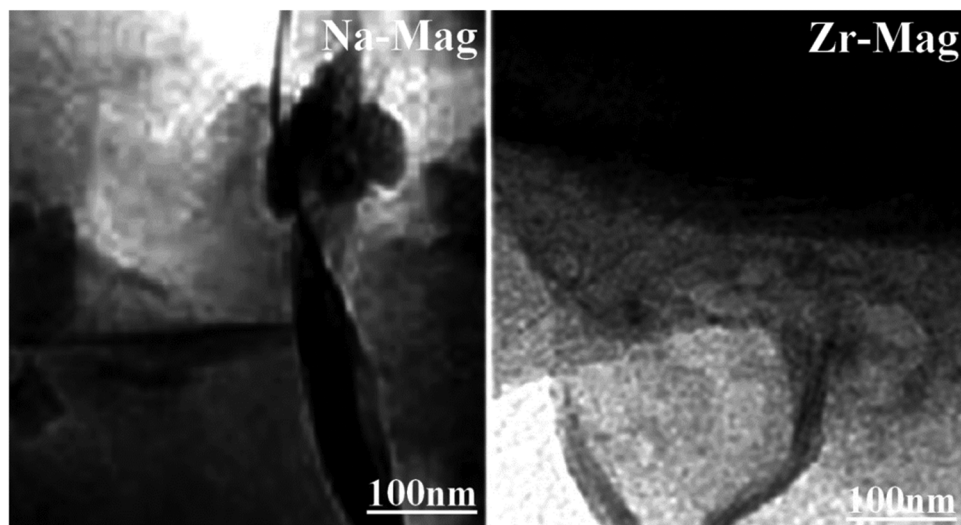
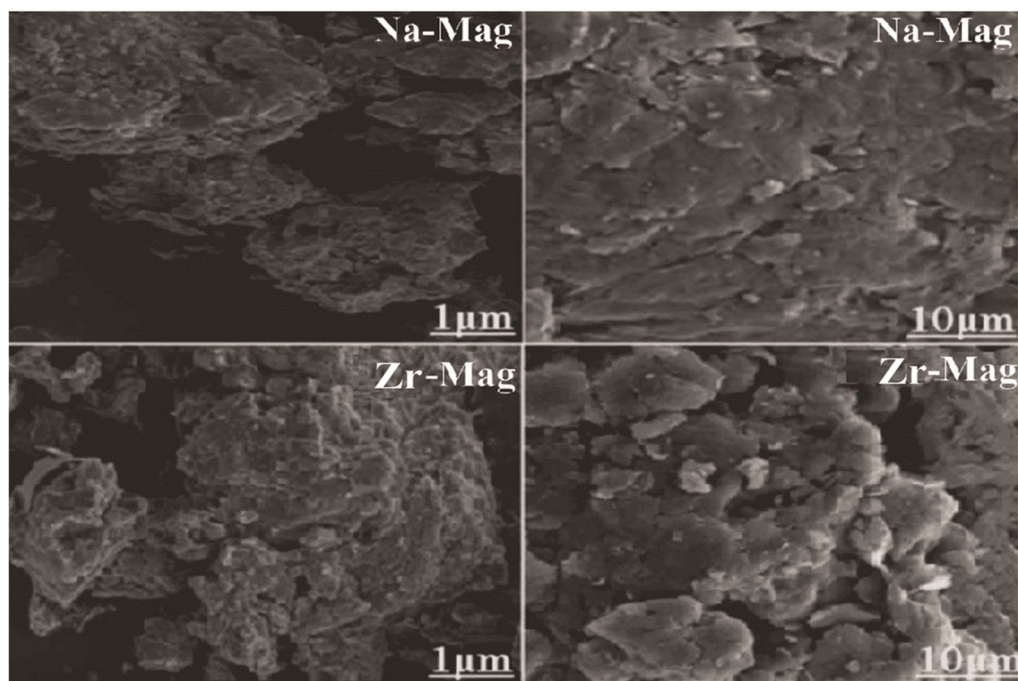Fig. 3 —TEM micrographs of Maghnite with Na-Mag and Zr-Mag interlayers.

Fig. 4 — SEM micrographs of Na-Mag and Zr-Mag.

layer by layer. While Zr-Mag revealed a nanoscale striped pattern, signaling an intercalated structure in which the zirconuim agent species are intercalated between the different Maghnite layers. These results are therefore consistent with the data obtained from the DRX analysis.

Scanning electron microscopy

Scanning electron microscopy (SEM) analyses of Na-Maghnite and Zr-Maghnite clays are shown in Fig. 4, which illustrates the morphological behavior and character of the homogenized Na-Mag and PNa-Mag clays. The observed particle size of Na-Mag is less than 10 μm in diameter. These particles have a flocculent, bulked, disordered appearance consistent with the lamellar, multi-layered structure of the clay (maghnite). SEM images indicated that the Maghnite structure was preserved following Zr-Na treatment.The grain size of the examined clays is around 2-10 μm. The intercalation phase only takes

place in the inter-lamellar space. This phenomenon explains the similarity of morphology between Na-Mag and Zr-Mag clays.

Thermo gravimetric analysis (TGA, DTA)

Figure 5 shows the thermal behaviour in the RT-1000°C range for sodium exchange montmorillonite (Na-Mag) and pillar montmorillonite (Zr-Mag). The overall profile of the thermal curve clearly shows two evolutions: the first, in the temperature range from RT to 200°C, and the second, in that of 200 to 900°C. In the case of Na-Mag, the first evolution can be attributed to the presence of physisorbic and hydrating water, while the second corresponds to a dehydroxylation of the structure of the silicate, which can sometimes occur in a dissociated form in two parts, barely visible in the measurement by ATG, but clearly visible in the proportional measurement of DTG (Fig. 6) at 597 and 666°C. Observing the TGA diagram (Fig.5), it
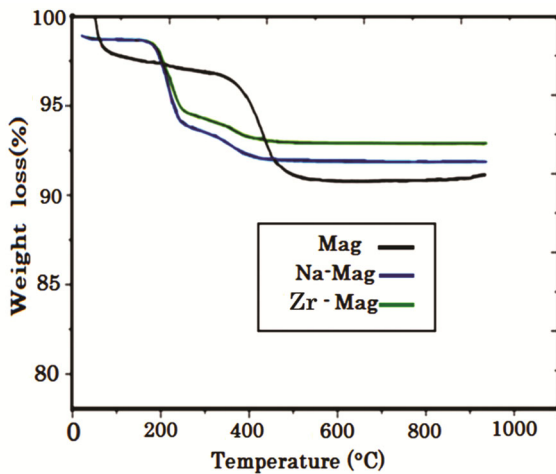
appears that the silicate structure is dehydroxylated in two distinct media, notably in the presence of Al and Mg, following the occurrence of a significant isomorphic substitution in the maghnite clay lattice, characterised by distinct bond strengths between Mt and nearby oxygen (or hydroxyl) ions[25].

Table 2 shows the mass losses corresponding to the different areas of Na-Mag and Zr-Mag.

The presence of hydroxy-Zr species and the hydroxyl groups involved in the water-water hydrogen bonds explains the large mass loss in the Zr-Mag samples [26], which is consistent with the IRTF data.

The main characteristic of the DTA curve for sodium maghnite corresponds to endothermic behaviours between RT and 200°C. These temperature ranges reflect the process of elimination of physisorbed water present on the external surface of the clay as well as that of water in the interlamellar space. During the second phase, the sodium montmorillonite undergoes dehydroxylation in several stages between 400 and 700°C .

Dynamic light scattering (DLS)

Figure 7 illustrates the behaviour of DLS in the distribution of Maghnite particle size. Most of these particles are in the size range of 1 to 900 nm. The particle size distribution is monomodal, peaking at 182 nm. In addition, the load rate of solid materials in the solution is a major parameter in the generation of the surface load. In order to determine how the solid/solution ratio affects zeta potential,

Fig. 5 — TGA curves of the Mag, Na-Mag and Zr-Mag .

Table 2 — Percent losses of the samples.			
Sample	25 –220^{0}C	220 – 900 ^{0}C	Total
Na -Mag	7.11 %	5.87 %	13.32 %
Zr -Mag	10.32 %	5.94 %	20.01 %

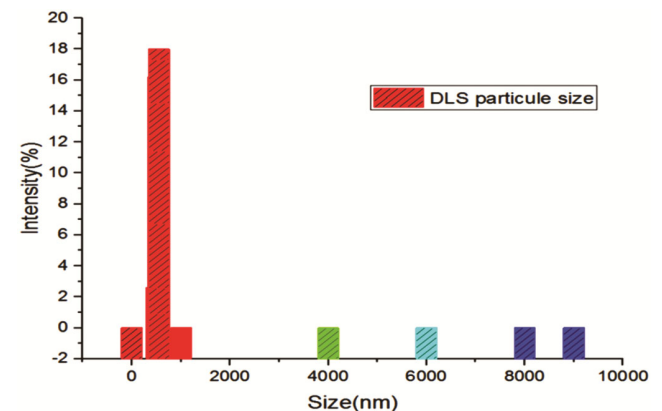Fig. 6 — DTG curves of the Mag, Na-Mag and Zr-Mag.

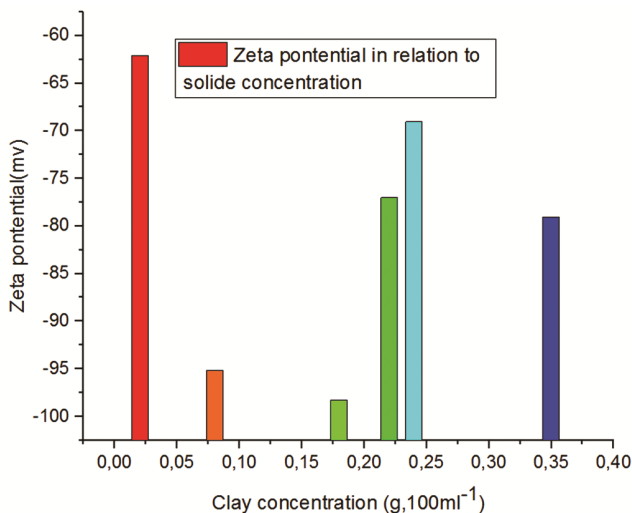

Fig. 7 — Characterization of DLS particle-size distribution

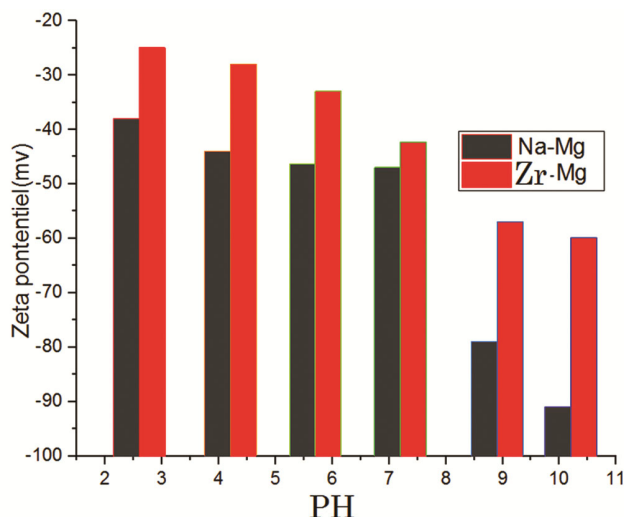Fig. 8 — Characterization of Zeta potential as a function of solid concentration.

Fig. 9 — Zeta potential values as a function of pH (1.5 g.L^{-1} clay suspensions).

concentrations of 0.05 to 0.3 (g.L^{-1}) were prepared in distilled water for different dispersions of montmorillonite from which zeta potentials were measured (Fig. 8). Clay samples (1.5 g.L^{-1}) showed an average zeta potential of -96.6 mV. The following experiments were performed in a solid/solution ratio of 1.5 g.L^{-1} (Ref. 27).

Figure 9 shows the zeta potentials of Zr-Mag and Mag in aqueous solutions with variable pH levels. Negative Na-Mag values remain stable across the pH range, indicating an extremely negative surface area. The shelling phase has a strong impact on the surface behaviour of Na-Mag. According to Clearfield [28], dissolution of the tetramer cations of type [Zr (OH)$_2$-
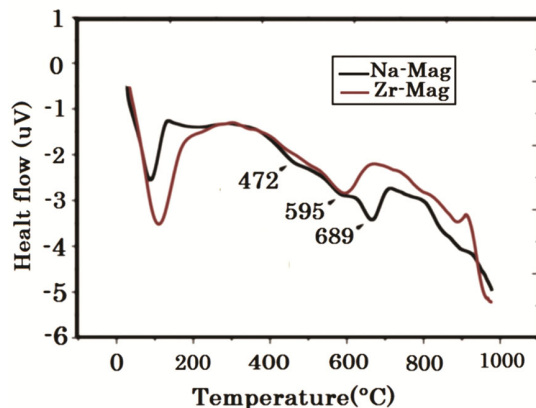

Fig.10 — DSC curves of the Na-Mag and Zr-Mag.

$4H_2O]_4)^{8+}$ in the solid phase of zirconium oxychloride causes their hydrolysis in aqueous medium in order to generate deprotonate species with a lower load with a pH of 2.7, the zero point of charge of the maghnite particles was not yet defined.

Differential Scanning Calorimetry (DSC)

Figure 10 shows the DSC curve of Na-Mag and Zr-Mag, which shows a maximum increase in Tg of 7.5°C of Zr-Mag compared to Na-Mag (472, 595, 689°C), The Tg values of Zr-Mag are higher than those of Na-Mag. This increase is the result of dehydroxylation from different media and interlamellar water loss.

Conclusion

The resulting modified Maghnites have been successfully obtained using zirconium pillars (Zr-Mag) from welded Maghnite (Na-Mag). FTIR and DRX analyses, TEM, SEM confirm that the structure of the zirconium pillar silicates has been obtained. The modification takes place via a cationic change due to the presence of intercalated zirconium ions in the lamellar structure of Na-Mag. The FT-IR and XRD results show that the ions of the zirconium pillars were intercalated, resulting in an intensification of the distance between the layers. In addition, the SEM and TEM reviews demonstrate the presence of layered distribution in the maghnite plates, revealing partial or total intercalation. Thermogravimetric measurements show that zirconium pillar species have a greater thermal stability than their Na-Mag counterparts. It has been established in this study that the surface charge of Maghnite exhibite a strongly negative zeta potential, a sign that this clay can be effectively exploited in the removal of cationic

species from water. The main objective of this work is the synthesis of zirconium pillars (Zr-Mag) from a green raw material (clay) as a catalyst and as a nanoscale filler in nanocomposite synthesis reactions.

References
1   Megherbi R, Mrah L & Marref M, *Iran Polym J*, 31 (2022) 223.
2   Khiati Z & Mrah L I, *J Chem Techn*, 29 (2022) 117. 3 Mrah L, *Polym Polym Compos*, 30 (2022) 09673911221080302.
3   Rathore B S, Chauhan N P S, Rawal M K, Rawal M K , Ameta S C & Ameta R, *Polym Bull*, 77 (2020) 4833.
4   Figueras F, *Catal Rev Sci Eng*, 30 (1988) 457.
5   Jozefaciuk G & Bowanko G, *Clays Clay Minerals*, 50 (2002) 771.
6   Clearfield A & Vaughan P A, *Acta Crystallogr*, 9 (1956) 555.
7   Cazotti J C, Salvato R C, Alves G M, Moreira J C & Santos A M, *Polym Bull*, 76 (2019) 6305.
8   Mrah L, Marref M & Megherbi R, *J Polym Eng*, 42 (2022) 57.
9   Jeldres M, Robles P, Toledo P G, Saldaña M, Quezada L & Jeldres R I, *Colloids Surfaces A: Physicochem Eng Asp*, 612 (2021) 126015.
10 Noel A, Mirbel D, Cloutet E, Fleury G, Schatz C, Navarro C & Hadziioannou G, *Appl Surf Sci*, 428 (2018) 870.
11 Sugimoto T, Adachi Y & Kobayashi M, *Colloids Surfaces A: Physicochem Eng Asp*, 632 (2022) 127795.
12 Mrah L & Meghabar R, *J Thermoplast Compos Mater*, 35 (2020) 1889.
13 Castellini E, Malferrari D, Bernini F, Brigatti M F, Castro G R, Medici L & Borsari M, *Clays Clay Min*, 65 (2017) 220.
14 Abhijit P, Sarat Chandra K, Partha M, Shubhamoy C & Rajarshi G, *Indian J Chem*, 56 (2017) 1317.
15 Lijun R & Chunlan Y, *Indian J Chem*, 57 (2018) 626.
16 Mrah L & Meghabar R, *Polym Bullet*, 78 (2021) 3509.
17 Zhuo H, Mei Z, Chen H & Chen S, *Polym*, 148 (2018) 119.
18 Mrah L & Meghabar R, *S N Appl Sci*, 2 (2020) 659.
19 Mrah L, Meghabar R & Belbachir M, *Bullet Chem React Eng Catal*, 10 (2015) 249.
20 Poonam Y, Shobhana S, Suman K, Seema & Mamta R, *Indian J Chem*, 60 (2021) 1539.
21 Vergnes B, *Polym Process*, 34 (2019) 482.
22 Duman O, Polat T G, Diker C Ö & Tunç S, *Int J Biol Macromol*, 160 (2020) 823.
23 Kundu D & Ganguli D, *J Mater Sci Lett*, 5 (1986) 293.
24 Mnasri S, Hamdi N, Frini-Srasra N & Srasra E, *Arab J Chem*, 10 (2017) 1175.
25 Salerno P & Mendioroz S, *Appl Clay Sci*, 22 (2002) 115.
26 Ladjal N, Zidelkheir B & Terchi S, *J Therm Anal Calorim*, 134 (2018) 881.
27 Zhang S, Liu Q, Gao F, Ma R, Wu Z & Teppen B J, *Appl Clay Sci*, 158 (2018) 204.